Available online at www.sciencedirect.com
ScienceDirect
Journal of Power Sources 174 (2007) 302–311
JOURNAL OF POWER SOURCES
www.elsevier.com/locate/jpowsour

Glass fiber entrapped sorbent for reformates desulfurization for logistic PEM fuel cell power systems

HongYun Yang, Yong Lu, Bruce J. Tatarchuk *

Department of Chemical Engineering, Auburn University, Auburn, AL 36849, USA

Received 6 July 2007; received in revised form 13 August 2007; accepted 13 August 2007
Available online 19 August 2007

Abstract

Glass fiber entrapped ZnO/SiO_2 sorbent (GFES) was developed to remove sulfur species (mainly hydrogen sulfide, H_2S) from reformates for logistic PEM fuel cell power systems. Due to the use of microfibrous media and nanosized ZnO grains on highly porous SiO_2 support, GFES demonstrated excellent desulfurization performance and potential to miniaturize the desulfurization reactors. In the thin bed test, GFES (2.5 mm bed thickness) attained a breakthrough time of 540 min with up to 75% ZnO utilization at 1 ppm breakthrough. At equivalent ZnO loading, GFES yielded a breakthrough time twice as long as the ZnO/SiO_2 sorbent; at equivalent bed volume, GFES provided a three times longer breakthrough time (with 67% reduction in ZnO loading) than packed beds of 1–2 mm commercial extrudates. GFES is highly regenerable compared with the commercial extrudates, and can easily be regenerated *in situ* in air at 500 °C. During 50 regeneration/desulfurization cycles, GFES maintained its desulfurization performance and structural integrity. A composite bed consisting of a packed bed of large extrudates followed by a polishing layer of GFES demonstrated a great extension in gas life and overall bed utilization. This approach synergistically combines the high volume loading of packed beds with the overall contacting efficiency of small particulates.

Keywords: H_2S removal; Microfibrous materials; ZnO sorbent; PEM fuel cells

1. Introduction

High efficiency desulfurization is critical to maintain the activities of fuel processing catalysts and high-value membrane electrode assemblies in logistic PEM fuel cell systems [1–4]. Metal oxides can be used to remove sulfur species from gas streams [5–13]. Among these studies, zinc oxide (ZnO) is widely applied to remove sulfur species such as H_2S from fuel gases because of its high-sulfur capacity and favorable sulfidation thermodynamics at moderate temperatures [14]. Traditional technology using packed bed reactors, given enough reactor volume, can successfully remove sulfur compounds from several thousand ppm to sub-ppm levels using metal oxide-based sorbents [1,2]. Commercial sorbents widely used in packed beds are of large particle sizes (ca. 1–5 mm), thus they normally demonstrate low-sorbent utilization and poor regenerability because of low contacting efficiency, intra-particle and lattice diffusion limitations [15]. As a result, packed beds with large reactor sizes are usually required to achieve low H_2S concentrations. In order to achieve high-efficiency sulfur removal, different approaches have been proposed. Rare metals and catalyst washcoats have been used to avoid one or more of these problems [16–19], but the surface areas per unit reactor volume still need further improvements. In a logistical fuel cell system, the overall system weight and volume are critical concerns. Therefore, the novel sorbent and reactor designs with high sorbent utilization, high capacity and miniaturized reactors are favored for logistic power systems.

Microfibrous media developed at the Center for Microfibrous Materials Manufacturing (CM^3) at Auburn University has demonstrated significant improvements in heat/mass transfer and regenerability [20–28]. This generic approach utilizes micro-sized fibers to entrap sorbent and catalyst particulates into sinter-locked structures with high voidage. Due to the improved contacting efficiency, these microfibrous materials can reduce both the reactor weight and volume. As for H_2S removal, Ni microfibrous entrapped sorbents were prepared and demonstrated a breakthrough time three times longer than a packed

* Corresponding author. Tel.: +1 334 844 2023; fax: +1 334 844 2065.
E-mail addresses: tatarbj@auburn.edu, brucet@eng.auburn.edu (B.J. Tatarchuk).

0378-7753/$ – see front matter © 2007 Elsevier B.V. All rights reserved.
doi:10.1016/j.jpowsour.2007.08.031

bed of commercial ZnO extrudates [3]. However, Ni fiber cannot withstand the highly oxidizing atmosphere used during sorbent regeneration. New microfibrous entrapped sorbents that are able to work in both reducing and oxidizing environments are required. In this study, glass fiber entrapped micro-sized supported-ZnO sorbent particulates were prepared for regenerable desulfurization applications for logistic PEM fuel cell power systems.

2. Experimental

2.1. Sorbents preparation and characterization

A series of supported-ZnO sorbents were prepared by incipient-wetness impregnation, using SiO_2 (300 $m^2\,g^{-1}$, mean pore size of 15 nm, Grace Davison) and γ-Al_2O_3 (150 $m^2\,g^{-1}$, mean pore size of 7 nm, Alfa) as supports. The detailed procedure for producing glass fiber entrapped sorbents is described by way of a sample preparation: 6 g of S2 glass fiber fibers (8 μm diameter) and 2 g of cellulose were added into water and stirred vigorously to produce a uniform suspension. The suspension and 18 g of 150–250 μm SiO_2 were added into a headbox of the 1.0 ft^2 M/K sheet former under aeration. The preform (1 ft^2) was then formed by vacuum filtration followed by drying on a heated drum. The glass fiber sheet was pre-oxidized in airflow for 30 min at 500 °C and then sintered for 1 h at a high temperature, ca. 900 °C. The prepared microfibrous entrapped SiO_2 was immersed into the zinc nitrate solution (2 mol L^{-1}) for 10 min, and subsequently vacuum drained and naturally dried overnight. Then it was calcined in air at 450 °C for 1 h.

Powder XRD patterns were recorded on a Rigaku MiniFlex II instrument using a scanning speed of 4° min^{-1} and an accelerating voltage of 40 kV, unless stated otherwise. SEM micrographs of the GFES were obtained by a Zeiss DSM 940 instrument. The ZnO loading on support was analyzed by ICP-AES using a Thermo Jarrell Ash ICAP 61 Simultaneous Spectrometer. The surface areas of the sorbents were measured by N_2-BET.

2.2. Gas and sample analysis

All gases in this work were purchased from Airgas South, Inc. Two sulfur source gases were employed in this paper: 2 vol.% H_2S–H_2 and 60 ppm H_2S in a model reformate stream (40 vol.% CO_2, 10 vol.% CO, 9 vol.% C_1–C_3 hydrocarbon, balance H_2). Other challenge gases (e.g., 5050 ppmv H_2S–H_2) were prepared by mixing 2 vol.% H_2S–H_2 with H_2. The outlet H_2S concentrations were analyzed by a Gow-Mac 550 GC equipped with a TCD detector (H_2 as the carrier gas) which was able to measure the H_2S concentration down to 200 ppmv. Gas samples were injected to the GC every minute by a 6-port-valve with a sampling loop of 50 μL. The whole sampling system was connected by 1/8″ tubing, and the pressure drop of this sampling system was negligible at all experimental conditions. Below 200 ppmv, the H_2S concentrations were measured by a Varian 3800 GC equipped with a pulse flame photometric detector (PFPD) capable of analyzing H_2S at sub-ppmv levels. Gas samples (250 μL) in low concentration tests were collected and injected manually.

3. Results and discussion

3.1. Commercial sorbent evaluation and supported sorbent design

In a preliminary experiment, a packed bed of commercial extrudates (3/16″, 16.50 g) containing 90 wt.% ZnO was tested with 5050 ppmv H_2S in H_2 at a face velocity of 20.3 cm s^{-1} and 400 °C. The dimensions of the packed bed were 2.14 cm diameter × 3.4 cm thickness. The test result, shown in Fig. 1, suggests that 70% ZnO in extrudates was accessible at 400 °C. Under the test conditions in Fig. 1, the packed bed failed to yield a H_2S concentration lower than 1 ppmv. At a higher breakthrough concentration of 50 ppmv (1% of inlet H_2S concentration C_0), the breakthrough time read from the breakthrough curve was 40 min, which suggests only 8% ZnO reacted with H_2S at the breakthrough under the test conditions. A further analysis showed that only the ZnO in a layer of 50 μm (average) from the outer surface was utilized prior to the breakthrough. ZnO particles with a size less than 100 μm should be fully utilized under the test conditions and the breakthrough concentration. In a similar study performed by Song et al. [2], only 3‰ ZnO was utilized at 0.1 ppmv breakthrough in the presence of 20% water. The layer thickness was calculated to be 0.2 μm (200 nm) in average, indicating that only nanosized ZnO particles could be fully utilized at the specified desulfurization application.

It is well known that small particle size can reduce the pore diffusion resistance and enhance the external mass transfer rate. Further tests on the commercial ZnO sorbents of various particle sizes were performed at 400 °C, and the results are shown in Fig. 2. The saturation capacity of the commercial sorbent increased with a decrease in particle size, and the breakthrough capacity followed the same trend, but not significantly.

Based on the results from Figs. 1 and 2, the nanosized particles would achieve complete utilization during desulfurization. Although the use of small particles promotes the mass transfer, it also introduces high pressure drop and bed channeling in packed beds, and sorbent particles with diameter less than 100 μm are not practically employed in packed beds, let alone nanosized sorbents. As a compromised design, nanosized ZnO particles or grains could be loaded on inert support particles, which can be used in packed beds or entrapped in microfibrous

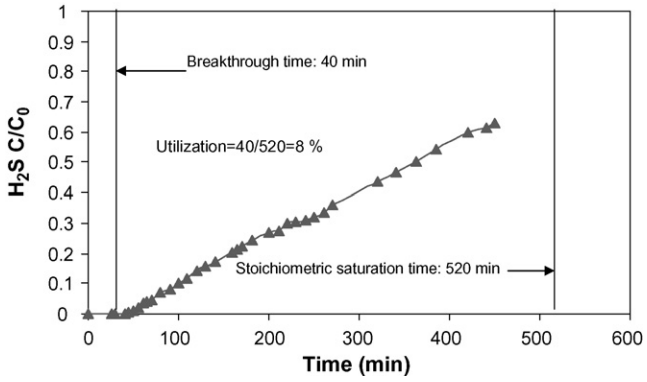

Fig. 1. Desulfurization performance of a commercial ZnO-based sorbent.

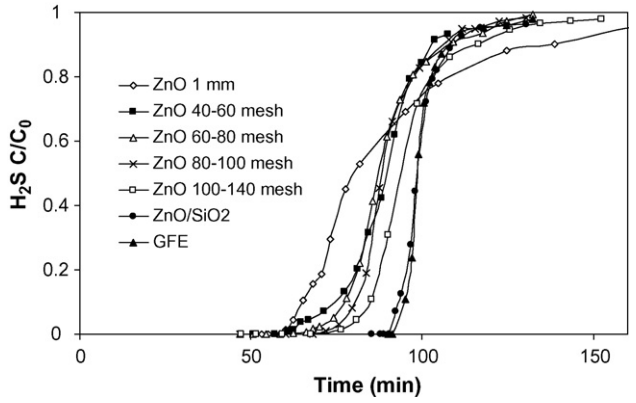

Fig. 2. Breakthrough curves of commercial ZnO sorbents with different size, and breakthrough curve of ZnO/SiO_2 sorbent is shown for comparison.

media. Supports with high porosity, small size and large surface area will be favored due to the reduced pore diffusion resistance and improved the intrinsic volumetric reaction rate. In addition to supporting ZnO, the inert support particles can stabilize ZnO [9,10], keep ZnO highly dispersed, inhibit the grain growth, and thus yield stable performance with extended service life.

3.2. Supported ZnO sorbents

3.2.1. Support screening

Three typical supports, SiO_2, Al_2O_3 and activated carbon particles (ACP), are widely employed in industries. ACP will react with oxygen during the regeneration of the spent sorbent; therefore, SiO_2 (40–60 mesh) and γ-Al_2O_3 (40–60 mesh) were chosen as supports for further evaluation. ZnO/SiO_2 and ZnO/Al_2O_3 sorbents were prepared at different calcinations temperatures and tested for H_2S removal at 400 °C. These two supports, according to preliminary experimental results, have negligible adsorption sulfur capacities at 400 °C.

Fig. 3 suggests that the H_2S adsorption performance of a supported ZnO sorbent strongly depends on the type of support and calcination temperature. As shown in Fig. 3, SiO_2 and Al_2O_3 supported ZnO sorbents demonstrated comparable sulfur capacity at a calcination temperature of 300 °C. However, the results at the calcination temperature of 500 °C are quite different. After calcination at 500 °C for 60 min, H_2S saturation capacity of SiO_2-supported ZnO sorbent remained almost unchanged, but that of γ-Al_2O_3-supported ZnO demonstrated a dramatic reduction. It is well known that the surface of γ-Al_2O_3 is quite reactive, but the surface of SiO_2 is very inert. Above 500 °C, a strong association or solid reaction between ZnO and γ-Al_2O_3 took place and an inactive "$ZnAl_2O_4$-like" compound was formed. The solid reaction was accelerated by the increase in calcination temperature leading to a rapid deactivation of γ-Al_2O_3-supported ZnO sorbent. Because ZnO-based sorbents are usually regenerated at a temperature above 500 °C, the result in Fig. 3 indicates that the Al_2O_3 supported ZnO sorbent will not maintain its performance after regeneration. Therefore, SiO_2 was chosen as the appropriate support for ZnO.

The calcination temperature also affects the performance of SiO_2-supported ZnO sorbent (ZnO/SiO_2). As shown in Table 1,

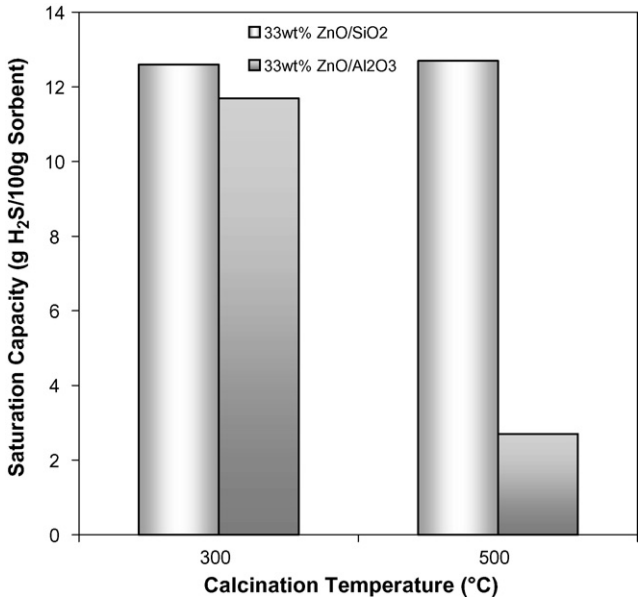

Fig. 3. Supports screening.

Table 1
Calculated grain size at different calcination temperatures using Debye–Scherrer equation

Calcination T (°C)	Grain size (nm)
350	1.25
450	2.90
600	2.98
752	3.60

Calcination time was 1 h.

ZnO grain size increases with the calcination temperature and regeneration temperature. Therefore, low calcination and regeneration temperatures are always preferred to retard grain growth.

3.2.2. ZnO loading effects

ZnO/SiO_2 sorbents with different ZnO loadings were prepared and their H_2S adsorption performances are displayed in Fig. 4. It shows that the H_2S adsorption capacity increased with the ZnO loading to 33 wt.% and then dropped dramatically with the ZnO loading up to 50 wt.%. The above results

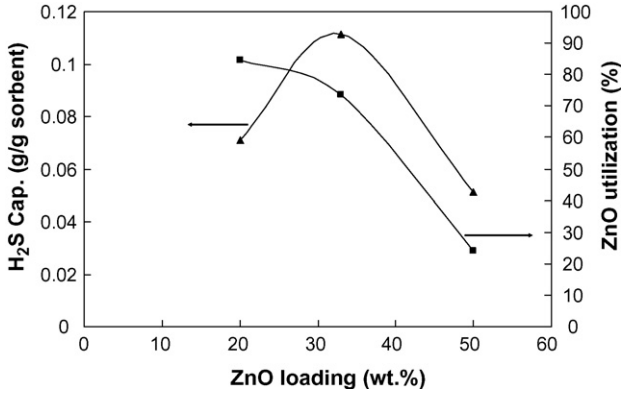

Fig. 4. ZnO loading ratio effects.

indicate that the optimal ZnO loading of ZnO/SiO_2 for high H_2S adsorption capacity is ~33 wt.% when zinc nitrate is used as the precursor of ZnO. ZnO utilization decreased sharply from 93% to 24% with an increase in ZnO loading in the range of 25–50 wt.%. The sorbent with a high capacity and the sorbent with a high ZnO utilization can be employed for different applications.

3.2.3. Glass fiber screening

As stated earlier, microfibrous entrapment can further enhance the sorbent performance. For instance, Ni fiber entrapped sorbents demonstrated a two to threefold longer breakthrough time for H_2S removal with 67% reduction in sorbent loading, compared with 1–2 mm commercial extrudates. However, Ni fiber was oxidized in the presence of oxygen during regeneration, and the sinter-locked network collapsed after 10 adsorption/regeneration cycles [3]. Therefore, other microfibrous materials that can withstand the highly reducing and oxidizing environments and high temperatures ($T > 600\,^{\circ}C$) will be considered as alternatives to Ni fibers. Glass fibers may be the most suitable fiber for this application. Several glass/ceramic fibers and their properties and chemical compositions are listed in Table 2.

Based on their thermal properties and availability, E- and S-type glass fibers were selected to fabricate the microfibrous media. Preliminary test results suggested that S2 fiber (an S type glass fiber, 8 μm diameter × 6 mm length, Advanced Glassfiber Yarns LLC) was able to be sintered above 900 °C, as shown in Fig. 5. E glass fiber (10 μm diameter × 6 mm length, Owens Corning) was able to be sintered around 800 °C.

3.2.4. Properties of sorbents

Sorbents were characterized by X-ray diffraction (XRD) and scanning electron morphology (SEM). The SEM images of S2-glass fiber entrapped ZnO/SiO_2 shown in Fig. 5 suggest that the glass fibers partially melted during sintering and formed a sinter-locked fibrous network, which entrapped the SiO_2 particulates. This network holds the particles and keeps them from being carried away by the gas flow. The XRD patterns of glass fiber entrapped sorbents, ZnO/SiO_2 sorbents and ZnO extrudates are shown in Fig. 6 for comparison. The XRD pattern of ZnO extrudates (pattern c in Fig. 6) demonstrates strong ZnO peaks at 2θ values of 31.2°, 34.0° and 35.8°, indicating the existence of large ZnO grains. Glass fiber entrapped sorbent and ZnO/SiO_2 sorbents only show three humps at the corresponding 2θ positions. This suggests that ZnO in these two sorbents may not have good crystallinity, provided the ZnO grains are in very small sizes. The grain sizes of ZnO extrudates and glass fiber entrapped ZnO/SiO_2 sorbent estimated by Debye–Scherrer equation were 17 nm and 5 nm, respectively.

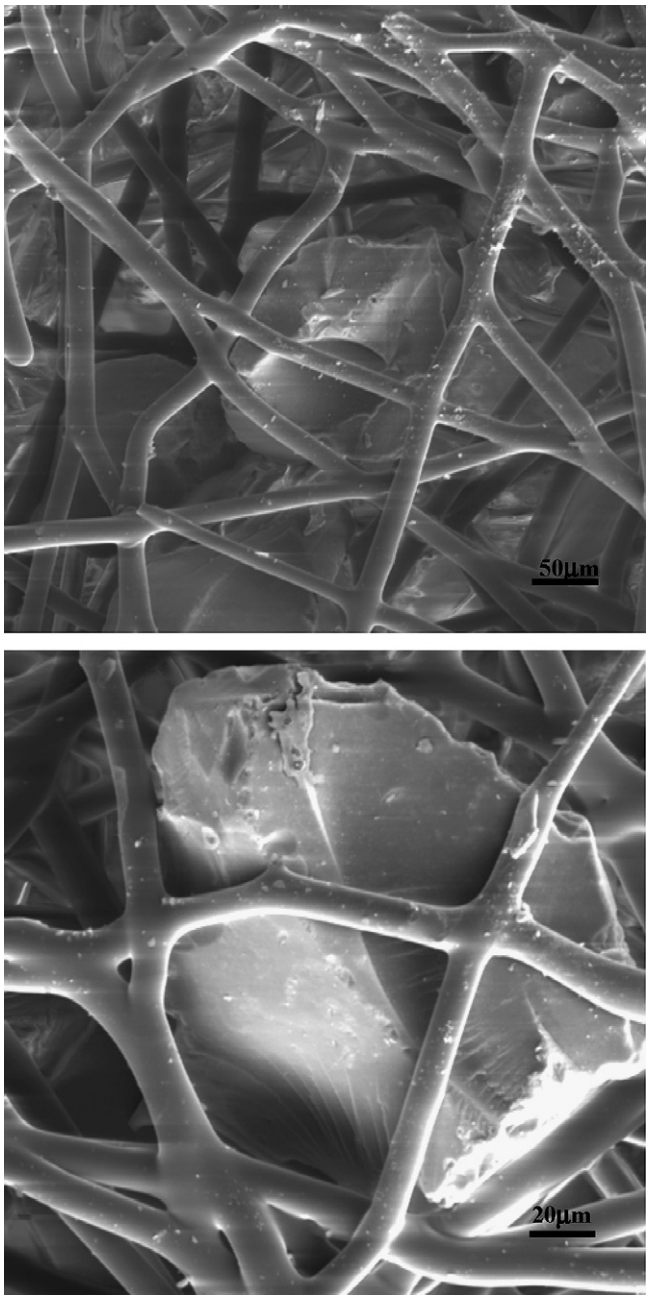

Fig. 5. Morphologies of S2 glass fiber entrapped ZnO/SiO_2.

Table 2
Properties of several glass fibers

	A-type	C-type	D-type	E-type	ECR-type	S-type	AR-type	R-type
Density (g cm^{-3})	2.44	2.52	2.11	2.58	2.72	2.46	2.7	2.54
Softening point (°C)	705	750	771	846	882	1056	773	952
Annealing point (°C)		588	521	657		810		
Strain point (°C)		552	477	615		760		

Curtsey of Owens corning [29].

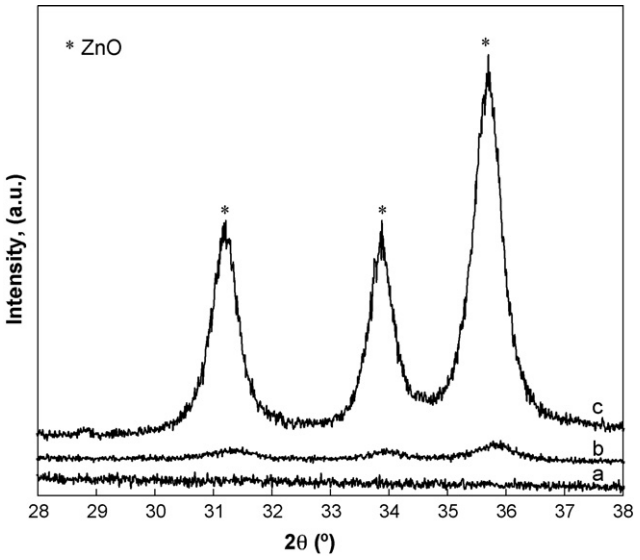

Fig. 6. XRD patterns of (a) GFE SiO_2, (b) GFE ZnO/SiO_2, and (c) commercial extrudates.

Other physical properties of glass fiber entrapped ZnO/SiO_2 sorbents were calculated and are shown in Table 3. The glass fibers occupy only 3 vol.%. Glass fiber entrapped ZnO/SiO_2 sorbents have a high-void fraction of 75 vol.%, which is about 2–2.5 times higher than that of a typical packed bed. As a result, the ZnO loading in the GFES (13 wt.%) is much less than that of the commercial ZnO extrudates (90–95 wt.%).

3.3. Pressure drop test

Zinc oxide extrudates were crushed and sifted into the desired sizes. The ZnO particles of each size range were loaded in a quartz reactor (10 mm diameter) and made into a packed bed with bed thickness (L) of 5 cm. Pure H_2 was passed through the packed bed at room temperature, and the total pressure drops (ΔP_t) at various face velocities were measured. The pressure drops introduced by the setup including the packing materials (ΔP_s) were also measured at the same velocities. The pressure drop generated by the packed bed (ΔP) equals ΔP_t minus ΔP_s. The pressure drop per unit bed thickness ($\Delta P/L$) of the packed bed at each face velocity was then calculated and plotted in Fig. 7. GFES was tested at the same conditions, and the data are also shown for comparison.

As shown in Fig. 7, the pressure drop increased with an increase in face velocity for every packed bed. Packed beds of smaller particles yielded higher pressure drop than larger

Table 3
Properties of glass fiber entrapped ZnO/SiO_2 sorbent

Component	wt.%	vol.%
ZnO	12	N.A.[a]
SiO_2	66	22[a]
Fiber	22	3
Void	N.A.	75

[a] ZnO was supported in the pores of SiO_2, and it did not change the size of SiO_2.

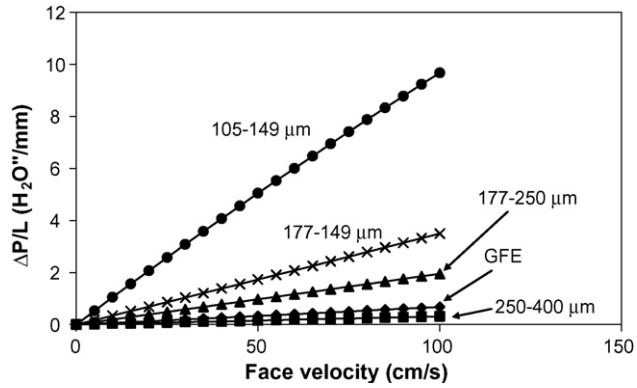

Fig. 7. Pressure drop per unit bed thickness at different face velocities for several desulfurization sorbents. Tested at room temperature using H_2 as challenge gas.

particle beds. For example, the 100–140 mesh (105–149 μm) particles yielded over 30 times larger pressure drop than the particles of 40–60 mesh (250–400 μm). The pressure drop per unit bed thickness of GFES (100–200 μm SiO_2 particles in 8 μm fibrous matrix) was two times greater than that of 40–60 mesh (250–400 μm) particles, and it is only 1/3 of that of 60–80 mesh (177–250 μm) particles at the same face velocity. It should be noted that both SiO_2 particle and fiber in GFES were smaller than the 60–80 mesh particles in the packed bed. The low-pressure drop over the GFES resulted from the high voidage (75 vol.%) of GFES.

3.4. Desulfurization test

3.4.1. High sulfur concentration test

In this study, all the ZnO/SiO_2 sorbents were tested at 400 °C with the challenge gas of 2 vol.% H_2S–H_2. In the experiment "m:v", 0.1 g of ZnO/SiO_2 sorbent was loaded in the reactor with a bed thickness of 2 mm at a gas face velocity of 1.2 cm s^{-1}. In the following experiments, the amount of sorbent loaded and the face velocity were doubled till the sorbent loading reached 0.8 g and face velocity reached 9.9 cm s^{-1}. All packed beds in this set of tests had the same stoichiometric saturation time (τ_s) of 12 min and the same residence time of 0.075 s (GHSV = 8100 h^{-1}). The breakthrough curves are shown

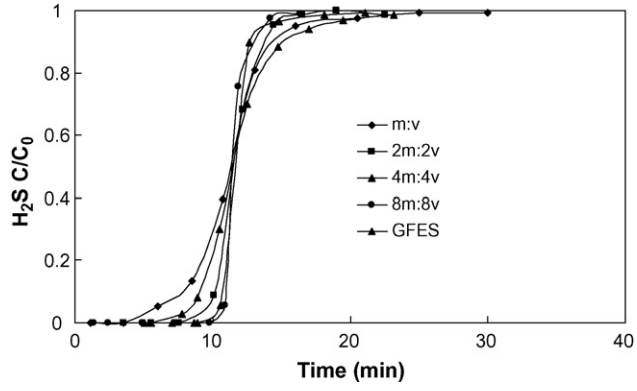

Fig. 8. Breakthrough curves for 2 vol.% H_2S–H_2 challenge gas at various face velocities (effects of glass fibrous media).

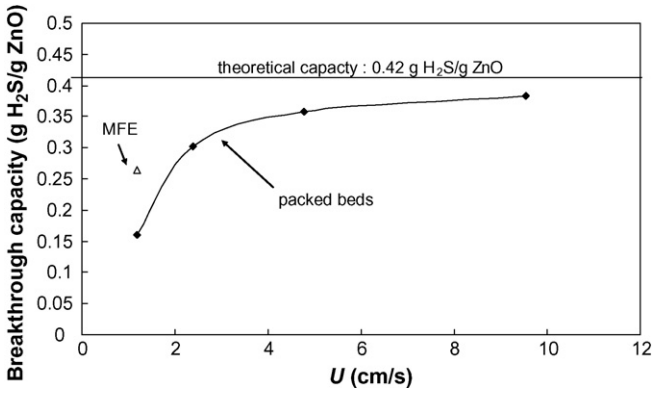

Fig. 9. Breakthrough capacity of ZnO/SiO_2 sorbent at different face velocities. Tested at 400 °C.

in Fig. 8. GFES containing 0.1 g of ZnO/SiO_2 sorbent was also tested at the velocity of 1.2 cm s^{-1} for comparison. The breakthrough sulfur capacities at 1% C_0 breakthrough for all experiments are shown in Fig. 9.

Due to the symmetry of the breakthrough curves, $t_{1/2}$, the time to reach 0.5 C_0, is close to the bed saturation time, τ. Therefore $t_{1/2}$ is used as the approximation of τ. As shown in Fig. 9, all the breakthrough curves pass around the same point (11.6, 0.5) in the time-C/C_0 plane, indicating the consistency of the saturation capacity. Moreover, the $t_{1/2}$ (or τ) is very close to τ_s. This suggests ZnO in ZnO/SiO_2 and GFES is completely accessible. It is a clear trend that the breakthrough curves become sharper with an increase in the face velocity of the challenge gas. The breakthrough capacity in each experiment was calculated and plotted in Fig. 9. The breakthrough capacity increases significantly in the low face velocity range. After the face velocity reaches 5 cm s^{-1}, the capacity slowly approaches 0.37 g H_2S/g ZnO, about 90% of the theoretical capacity, which suggests that the unutilized ZnO is less than 10% and a further increase in the face velocity is not necessary at this GHSV. The breakthrough curve of GFES shows that the breakthrough capacity increased about 50% compared with the packed bed experiment "m:v" in which the same type of sorbent (ZnO/SiO_2) with the same amount of ZnO was loaded. The only explanation for this improvement is the enhancement due to the using of glass fiber media.

3.4.2. Low sulfur concentration test

Similar tests were performed at a low-H_2S challenge concentration. The adsorption with a H_2S challenge of 60 ppmv in a model reformate stream (60 ppm H_2S–10 vol.% CO–40 vol.% CO_2–9 vol.% C_1–C_3 and H_2 balance) with 30 vol.% steam added at 400 °C was studied over both GFES and the commercial extrudates. The face velocity was 3.9 cm s^{-1} (GHSV = 27500 h^{-1} based on dry gas). The breakthrough H_2S concentration was defined at 1 ppm. The results are summarized in Table 4. GFES with a thickness of 2.5 mm yielded a breakthrough time of 540 min. At an equivalent bed volume, GFES provides a three times longer breakthrough time with a 67% reduction in sorbent loading than packed bed of 1–2 mm commercial extrudates. Compared with that of ZnO particles (80–100 mesh, 149–177 μm), the breakthrough time is 1.5 times longer. ZnO utilization in GFES was 75%, which is 14-fold higher than that of 1–2 mm extrudates.

Table 4
Comparison between GFE and commercial ZnO extrudate[a]

Sorbent	GFE ZnO/SiO_2	80–100 mesh ZnO	1–2 mm ZnO
Total weight (g)	0.2	0.55	0.55
ZnO content (mg)	34	495	495
Breakthrough time[b] (min)	540	350	180
ZnO Utilization at BT[c] (%)	74.1	3.3	1.7

[a] Tested at equivalent bed volume of 0.53 cm^3 (1.62 cm diameter × 0.25 cm thickness).
[b] Breakthrough time at 1 ppmv H_2S breakthrough.
[c] BT: breakthrough.

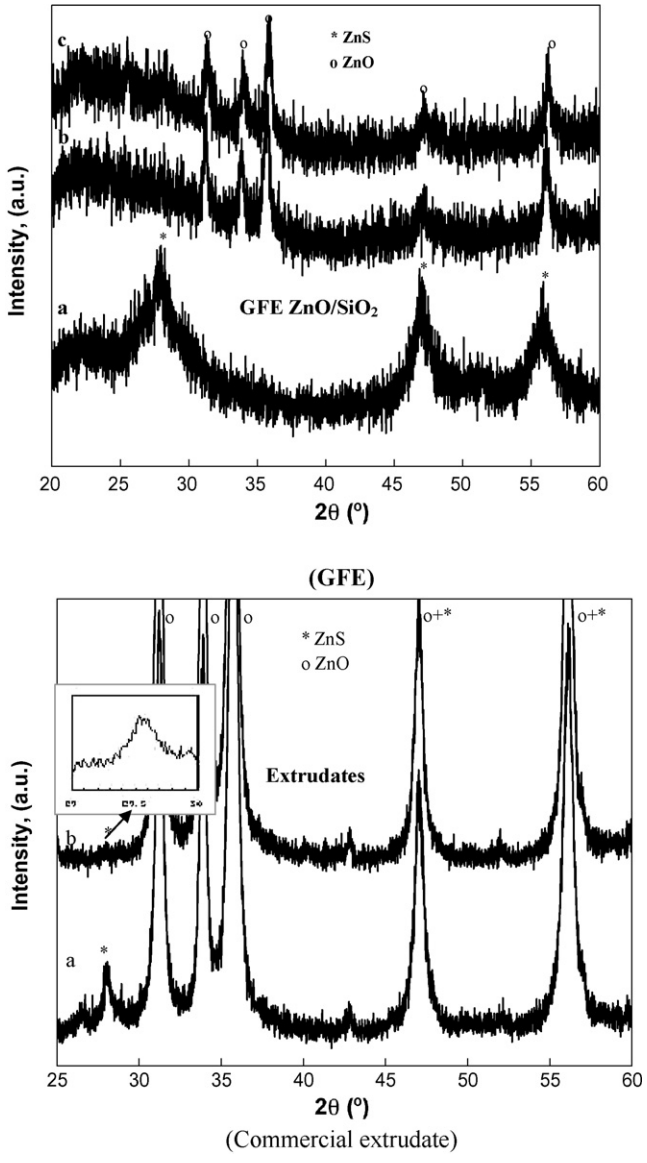

Fig. 10. XRD patterns of GFE ZnO/SiO_2 and commercial extrudates. (a) Spent, after regeneration in air at (b) 600 °C for 1 h and (c) 500 °C for 3 h.

XRD patterns of GFES and the commercial extrudates are shown in Fig. 9 (fresh sorbents) and Fig. 10 (spent sorbents). The results in Fig. 10 suggest that no ZnO crystal existed in the spent sorbent of GFES, and it was completely converted into ZnS. In extrudates, ZnO grains had a size of 17 nm, which is three times larger than those in GFES. In addition, the commercial extrudate sample had a BET surface area of ~25 $m^2 g^{-1}$, which is 10% of that of GFES. This suggests that most ZnO crystals were buried inside the bulk, and ZnO in GFES was highly dispersed. The size of the extrudates was around 1 mm, six times larger than that of ZnO/SiO_2 particles in GFES. These differences suggest the mass transfer resistances in extrudates due to lattice diffusion and pore diffusion should be much higher than those in GFES. As a result, ZnO grains in ZnO extrudates were not completely accessible to H_2S, and ZnO still existed and demonstrated strong ZnO peaks as shown in Fig. 10.

3.5. Regeneration test

3.5.1. Single cycle test

The nano-dispersed nature of ZnO and the use of small size support particulates significantly improved the desulfurization performance; they should also improve the regenerability of GFES. Satisfactory regenerability corresponds to high-regenerable capacity and short regeneration time. Table 5 compares the GFES with packed beds of the commercial ZnO extrudates and ZnO particles (80–100 mesh). From the breakthrough time (capacity) recovery percentage of GFES at different regeneration conditions, it is safe to conclude that higher regeneration temperature and longer regeneration time yields higher recovery percentage. This conclusion is also true for commercial ZnO sorbents. Under the same regeneration conditions (in air at 500 °C for 1 h), GFES, as expected, provided 10 times higher capacity recovery compared with the packed bed of the commercial extrudates. Under these conditions, the bed made of ZnO particles (80–100 mesh) also demonstrated good performance with ~60% capacity recovered. However, the breakthrough times of the bed were only 50% of those of GFES tested under the same conditions.

Regeneration time is an important concern for reactor design, especially for a system consisting of several reactors—one reactor is doing desulfurization and the others are being regenerated. For a shorter regeneration time, fewer reactors are required for continuous operation. For example, if the breakthrough time of a fixed bed desulfurization reactor is 1 h and the regeneration time for each reactor is 3 h, then four identical reactors are required. If the regeneration time can be reduced to 1 h, then only two reactors are required, and the total desulfurization reactor volume (or weight) is reduced to 50% of that in the earlier scenario. From the regeneration tests of GFES, the best regeneration condition for the sorbents is at 600 °C for 1 h. This condition yielded a good balance between regeneration time and recovery rate. Therefore, GFES were regenerated at this condition for the following cyclic tests.

To reveal the nature of this significant difference in regenerability, XRD analyses were carried out on spent samples before and after regeneration at 500–600 °C. The spent samples were collected when the outlet H_2S concentration reached 60 ppmv (the same as inlet concentration). As shown in Fig. 10, cubic ZnS was the only detectable phase on the spent GFES. After regeneration at 600 °C for 1 h or at 500 °C for 3 h in air, the ZnS phase completely disappeared and the ZnO phase appeared again. In the case of ZnO extrudate, ZnO was the predominant phase for the spent 1–2 mm commercial extrudates. ZnS phase was still detectable after 1 h regeneration at 600 °C in air (confirmed by XRD using a scanning speed of 0.1° min^{-1} and a sampling interval of 0.01 min). The comparison above suggests the supported sorbent design facilitates the regeneration. In Fig. 10, the regenerated GFES demonstrated a sharp ZnO peak with a corresponding grain size of 12 nm. Compared with the grain size (5 nm) of fresh sorbent, this is a significant increase.

3.5.2. Multiple cycle tests

Fig. 11 shows the desulfurization/regeneration cycle test results for the GFES. All of the desulfurization tests were conducted at 400 °C using the same experimental condition as described in Table 5; all regeneration experiments were carried out at 600 °C for 1 h *in situ* in an airflow of 200 mL min^{-1} (STP). Fig. 11 suggests that a significant breakthrough time (capacity) drop occurred after the first regeneration, and breakthrough times (capacities) remained almost unchanged through 50 absorption/regeneration cycles. Grain sizes of ZnO were calculated from the XRD pattern and are shown in Fig. 12. The grain size increased drastically from 5 nm to 12 nm after the first regeneration, and increased to 15 nm after the 50th cycle which is not a significant change compared with 12 nm after the first cycle. This grain growth is a common phenomenon for most sorbents that are regenerated at high temperatures. It is also well

Table 5
Capacity recovery percentage (C.R.) after regeneration at 500–600 °C in air[a]

Sorbent	GFE ZnO/SiO_2		80–100 mesh ZnO		1–2 mm ZnO	
	B.T.[b] (min)	C.R.[c] (%)[c]	B.T.[b] (min)	C.R.[c] (%)[c]	B.T.[b] (min)	C.R.[c] (%)
Fresh	540	–	350	–	180	–
1 h Regn.@600 °C	400	74	220	63	100	56
3 h Regn.@500 °C	410	76	210	60	80	44
1 h Regn.@500 °C	300	56	60	17	10	5.5

[a] Absorption experiment was carried out at 400 °C and 3.9 cm s^{-1} face velocity in the present of 30% steam, using 60 ppmv H_2S challenge in a model reformate.
[b] Breakthrough time at 1 ppmv breakthrough for H_2S.
[c] Percentage of capacity recovered, defined as: 100 (breakthrough time of regenerated sample/breakthrough time of fresh sample test).

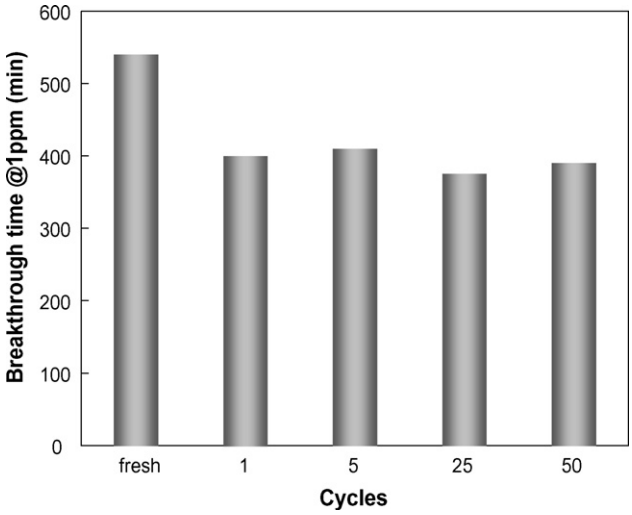

Fig. 11. Breakthrough time *vs*. regeneration cycle numbers.

known that the grain size increases significantly after the first regeneration. Undoubtedly, the significant increase in ZnO grain size after the first regeneration cycle resulted in severe lattice diffusion resistance, which in turn decreased the ZnO utilization, as observed in the reduction in breakthrough time for GFES. The ZnO grains did not grow above 15 nm possibly because the small pores of the SiO_2 support inhibited grain growth and made ZnO grain highly dispersed. As a result, the breakthrough time of GFE ZnO/SiO_2 during the multiple-cycle tests was stabilized around 400 min, as shown in Fig. 11. Moreover, the SEM image in Fig. 13 shows that the sinter-locked micro-glass structure of the microfibrous sorbent remained robust without any rupture after 50 regeneration cycles. This suggests that the glass fiber media has good thermal and structural stability for regenerable applications.

3.6. Composite bed

Although microfibrous entrapped sorbents, as mentioned earlier, demonstrated high ZnO utilization and high contacting

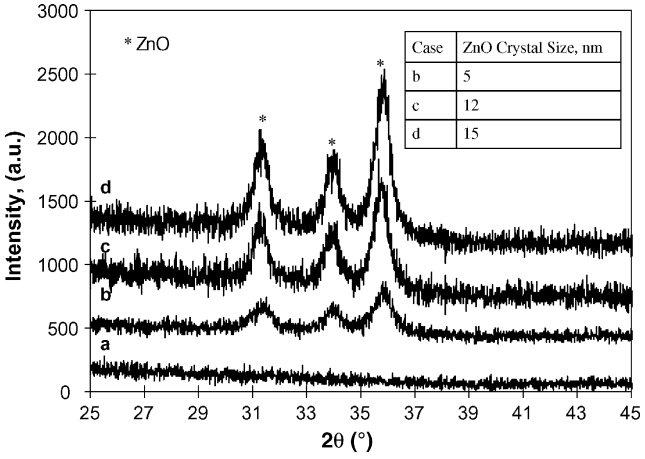

Fig. 12. XRD patterns of (a) GFE SiO_2 carriers and GFE ZnO/SiO_2 sorbents: (b) fresh, and after (b) 1st regeneration cycle and (c) 50th regeneration cycle. Regeneration was carried out in air at 600 °C for 1 h in each cycle.

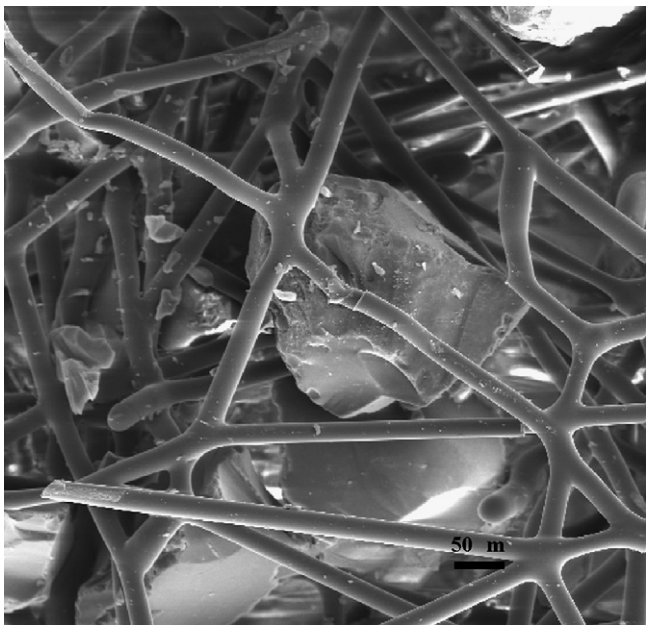

Fig. 13. Structure integrity after 50 cycles (SEM image).

efficiency, they do not have high ZnO loadings and their stoichiometric sulfur capacities are low. As a result, microfibrous entrapped sorbents may not be directly applied to remove H_2S at high concentrations, but their high contacting efficiency allows them to be applied in low-concentration H_2S removal. For example, microfibrous entrapped sorbents can be used as a polisher to remove trace H_2S from a packed bed. This unique approach offers opportunities for higher absorption capacity design by incorporating microfibrous entrapped sorbents as a polishing sorbent layer to back up a packed bed. This approach is described as a composite bed, as shown in Fig. 14.

The desulfurization performance of a packed bed and the corresponding composite bed is shown in Fig. 15. The tests were conducted in a quartz tube reactor (diameter 2.14 cm) with 5000 ppmv H_2S–H_2 challenge gas at a face velocity of 10 cm s^{-1} at 400 °C. The polishing layer was made of GFES (0.9 g) with a thickness of 5 mm and a ZnO loading at 13 wt.%. The packed bed was made of 3/16″ extrudates (11 g) with a bed thickness of 2.2 cm. The composite bed had an overall thickness of 2.7 cm.

As shown in Fig. 15, the bed of the commercial extrudates yielded a broad breakthrough curve and a breakthrough time around 33 min at 1 ppmv breakthrough as indicated in Fig. 16. After adding the polishing layer at the end of the packed bed, the breakthrough curve became sharper at low outlet H_2S concentrations, and the composite bed yielded a breakthrough time

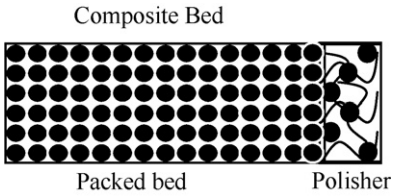

Fig. 14. A composite bed.

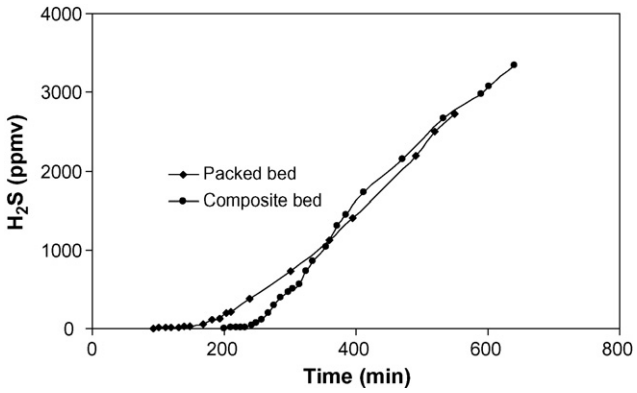

Fig. 15. Breakthrough curves of a 2″ thick packed bed of ZnO extrudates and a composite bed (the packed bed followed with a 5 mm polishing layer).

around 185 min at 1 ppmv breakthrough. The breakthrough time increased six times by adding the thin polishing layer at 25 vol.% of the packed bed, and the sulfur capacity per unit volume of reactor increased by 4.5 times. If the regeneration time for the composite bed is less than 3 h (180 min) and the composite bed can be regenerated for unlimited times, then two composite beds can continuously provide H_2S-free reformates.

It is obvious that GFES cannot add two times higher saturation capacity to the packed bed due to the low ZnO weight loading. However, GFES can reduce the H_2S concentration in the gas flow from the packed bed, which was much less than 5000 ppmv, to lower concentrations (less than 1 ppmv). The polishing layer did not capture more sulfur than the packed bed, but it was able to capture the H_2S at low concentrations more efficiently than the extrudates. Increasing the volume of the extrudate bed can also extend the breakthrough time by six times. However, due to the poor contact efficiency of big extrudates, a large amount of extrudates is required, which is a penalty in logistic power systems. In this case, the thin polishing layer with high contacting efficiency is the best choice to increase the breakthrough time (capacity) without significant increase in the reactor volume.

The polishing layer can improve the breakthrough time (capacity) more significantly, if the breakthrough curve of the packed bed is broader or the breakthrough concentration is lower, e.g. the desulfurization for reformates, in which CO, CO_2 and water yield broad breakthrough curves. As shown in Fig. 16, if the breakthrough is defined as 1% of challenge H_2S concentration (50 ppm), the breakthrough time of the packed bed and composite bed are 150 min and 220 min. This is only a 1.5 times improvement at 50 ppm breakthrough, compared with the six times improvement at 1 ppm breakthrough. This phenomenon can also be explained by the service time equation [30].

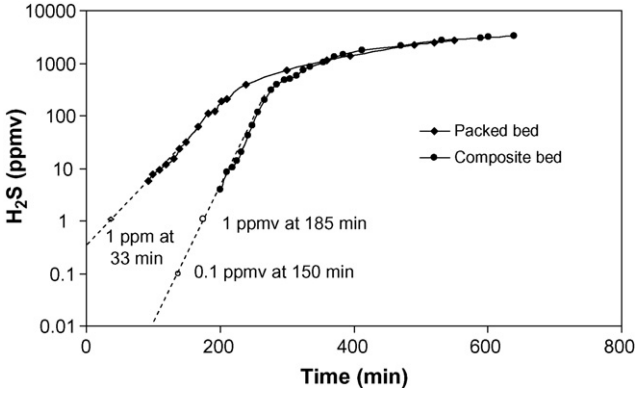

Fig. 16. Breakthrough curves of a 2″ thick packed bed of ZnO extrudates and a composite bed (the packed bed followed with a 5 mm polishing layer) in logarithmic scale.

$$\ln\left(\frac{C_0}{C} - 1\right) = K(\tau - t) \quad (1)$$

where C_0 is the H_2S concentration in the challenge gas, C the H_2S concentration at outlet of a packed bed, K is an experimental constant, τ the saturation time of the bed and t is the onsite time. According to Eq. (1), at a very low H_2S concentration, C can be expressed as

$$\ln(C) = \ln(C_0) - K(\tau - t) \quad (2)$$

Eq. (2) suggests the plot of $\ln(C_0)$ *versus* t in the low-H_2S concentration region should be linear. Extending the line of $\ln(C_0) - t$ plot to lower concentrations (ca. 0.1 ppmv), yields a breakthrough time at a new breakthrough concentration, as shown in Fig. 16. By adding the polishing layer (5 mm thickness) at the end of the packed bed of ZnO extrudate (2.2 cm thickness), Fig. 16 predicts the improvements at 200 min, 152 min and 70 min for 0.1 ppmv, 1 ppmv and 50 ppmv breakthrough, respectively.

4. Conclusions

Glass microfibrous entrapped ZnO/SiO_2 sorbent was designed and prepared for reformates desulfurization for logistic PEM fuel cell systems. It consist of 3 vol.% glass fibers, 22 vol.% entrapped 150–250 μm ZnO/SiO_2 sorbent particulates and 75 vol.% void. The microfibrous media made it possible to employ small sorbent and catalyst particulates in desulfurization process without introducing high-pressure drop and channeling. ZnO was nano-dispersed on the high-surface area SiO_2 support. This combination made the ZnO accessible during the desulfurization process, and also facilitated the regeneration of spent sorbent (ZnS/SiO_2) at 500–600 °C. Glass fiber solved the issues encountered in regeneration of Ni fiber entrapped ZnO/SiO_2. The glass fiber matrix was inert to most reducing and oxidizing environments and demonstrated good structural integrity after 50 desulfurization/regeneration cycles.

Due to the low ZnO loading, GFES can work independently for low-concentration H_2S removal. It also can be applied as a polisher in composite bed design approach. The combination of high-sulfur capacity of extrudates in a packed bed and high-contacting efficiency of microfibrous entrapped sorbents demonstrated significant improvements in the overall bed capacity and efficiency, compared with the packed beds alone. This approach provides a solution to minimize the volume of reactors in logistic fuel cell applications.

Acknowledgements

This work was supported by the US Army under a U.S. Army contract at Auburn University (ARMY-W56HZV-05-C0686) administered through the US Army Tank-Automotive Research, Development and Engineering Center (TARDEC). Authors want to thank Mr. Noppadon Sathitsuksanoh for characterizing the sorbents in this study. Authors also wish to thank Ms. Priyanka Dhage, and Mr. Sachin Nair who read the draft of the manuscript and provide helpful suggestions and comments.

References

[1] J. Larminie, A. Dicks, Fuel Cell Systems Explained, John Wiley and Sons, Ltd., New Jersey, 2002, pp. 181–249.
[2] I. Novochinskii, C. Song, X. Ma, X. Liu, L. Shore, J. Lampert, R.J. Farrauto, Energy Fuels 18 (2004) 576–583.
[3] Y. Lu, N. Sathitsuksanoh, H.Y. Yang, B.K. Chang, A.P. Queen, B.J. Tatarchuk, in: Y. Wang, J.D. Holladay (Eds.), ACS Symp. Ser., vol. 914. Microreactor Technology and Process Intensification, Washington, DC, 2005, pp. 406–422.
[4] J. Heinzel, A. Nickens, D. Hoffman, M. Cervi, Prepr. - Am. Chem. Soc., Div. Pet. Chem., 51 (2006) 502.
[5] P.R. Westmoreland, D.P. Harrison, Environ. Sci. Technol. 10 (1976) 659–661.
[6] E. Sasaoka, T. Ichio, S. Kasaoka, Energy Fuels 4 (1992) 603–608.
[7] R. Ben-Slimane, M.T. Hepworth, Energy Fuels 8 (1994) 1175–1183.
[8] T. Baird, P.J. Denny, R. Hoyle, F. McMonagle, D. Stirling, J. Tweedy, J. Chem. Soc., Faraday Trans. 88 (1992) 3375–3382.
[9] R. Gupta, S.K. Gangwal, S.C. Jain, Energy Fuels 6 (1992) 21–27.
[10] S. Lew, K. Jothimurugesan, M. Flytzani-Stephanopoulos, Ind. Eng. Chem. Res. 28 (1989) 535–541.
[11] R.B. Slimane, J. Abbasian, Adv. Environ. Res. 4 (2000) 147–162.
[12] L. Alonso, J.M. Palacios, E. Garcia, R. Moliner, Fuel Process. Technol. 62 (2000) 31–44.
[13] L. Kundakovic, M. Flytzani-Stephanopoulos, Appl. Catal. A: Gen. 171 (1998) 13–29.
[14] E. Sasaoka, Energy Fuels 8 (1994) 1100–1105.
[15] M.V. Twigg, Catalyst Handbook, 2nd ed., Wolfe, London, 1989, p. 209.
[16] T. McCreedy, Trends Anal. Chem. 19 (2000) 396–401.
[17] R. Srinivasan, I.M. Hsing, P.E. Berger, K.F. Jensen, S.L. Firebaugh, M.A. Schmit, M.P. Harrold, J.J. Lerou, J.F. Ryley, AIChE J. 43 (1997) 3059–3069.
[18] K. Watanabe, M. Sakairi, H. Takahashi, K. Takahiro, S. Nagata, S. Hirai, J. Electrochem. Soc. 148 (2001) B473–B481.
[19] X. Wu, D. Weng, L. Xu, H. Li, Surf. Coat. Technol. 145 (2001) 226–232.
[20] R.A. Overbeek, A.M. Khonsari, Y.-F. Chang, L.L. Murrell, B.J. Tatarchuk, M.W. Meffert, US Patent 6,231,792, 2001.
[21] S. Ahn, B.J. Tatarchuk, J. Appl. Electrochem. 27 (1997) 9–17.
[22] D.R. Cahela, B.J. Tatarchuk, Catal. Today 69 (2001) 33–39.
[23] D.K. Harris, D.R. Cahela, B.J. Tatarchuk, Compos. Part A: Appl. Sci. Manuf. 32A (2001) 1117–1126.
[24] D.A. Kohler, J.N. Zabasajja, A. Krishnagopalan, B.J. Tatarchuk, J. Electrochem. Soc. 137 (1990) 136–141.
[25] C.J. Marrion, D.R. Cahela, S. Ahn, B.J. Tatarchuk, J. Power Sources 47 (1994) 297–302.
[26] M.W. Meffert, Ph.D. Thesis, Auburn University, Auburn, AL, 1998.
[27] B.J. Tatarchuk, US Patent 5,096,663, 1992.
[28] B.J. Tatarchuk, US Patent 5,102,745, 1992.
[29] D.R. Hartman, M.E. Greenwood, D.M. Miller, High Strength Glass Fibers, Technical paper of Owens Corning, 1994.
[30] Y.H. Yoon, J.H. Nelson, Am. Ind. Hyg. Assoc. J. 45 (1984) 509–516.